Chapter 3

Application of Composite Right/Left-Handed Metamaterials in Leaky-Wave Antennas

Keyhan Hosseini and Zahra Atlasbaf

Additional information is available at the end of the chapter

http://dx.doi.org/10.5772/65643

Abstract

This chapter reviews the most significant advancements in the context of metamaterial (MTM) leaky wave antennas (LWAs). A brief review of the mechanism of leaky wave radiation along with an important class of MTMs known as composite right/left-handed (CRLH) structures is presented. Then, recent outstanding works in the area of CRLH LWAs are reported in detail. These works include the application of electronic control, substrate integrated waveguides, dual band and wideband performance, ferrite loaded waveguides, and split-ring-resonator (SRR)-based MTMs in LWAs. Also, the benefits of LWAs to design high gain active structures, reflecto-directive systems, wideband dual-layer substrate integrated waveguide antennas and conformal antennas are discussed.

Keywords: composite right-left handed (CRLH), dispersion diagram, leaky wave antenna (LWA), metamaterial (MTM), transmission line (TL)

1. Introduction

A leaky wave is a traveling wave progressively leaking out power as it propagates along a waveguiding structure. A leaky wave antenna (LWA) supports leaky waves where the leakage phenomenon is generally associated with high directivity [1]. LWAs are different from resonating antennas, as they are based on traveling waves as opposed to resonate-wave mechanism. Hence, their size is not related to the operation frequency, but to directivity [2]. A schematic LWA is depicted in **Figure 1**. If the wave is faster than the velocity of light ($\beta < k_0$), k_y is real and the leakage radiation occurs. This wave is called a fast wave. In this case, β determines the angle θ_{mb} of radiation of the main beam and as illustrated in **Figure 1**, follows the simple angle-frequency relation [1].

$$\theta_{mb} = \sin^{-1}\left(\beta / k_0\right) \tag{1}$$

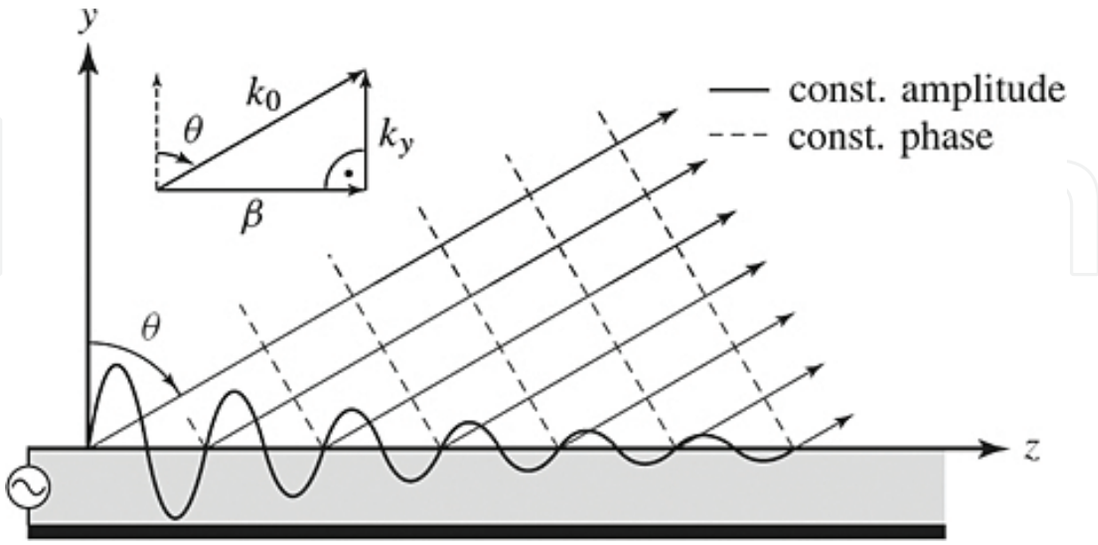

Figure 1. A general schematic LWA. The solid and dashed lines represent the constant amplitude and constant phase planes, respectively [3].

The values $\beta < 0, \beta = 0,$ and $\beta > 0$ correspond to backward, broadside and forward angles, respectively. If the waveguide is dispersive (β is a nonlinear function of ω) the main beam angle is changed as a function of frequency, $\theta_{mb} = \theta_{mb}(\omega)$. This phenomenon is called *frequency scanning*. Eq. (1) also reveals that radiation in any angle from backfire ($\theta_{mb} = -90$ °) to endfire ($\theta_{mb} = +90$ °) can be potentially achieved if β varies from $-k_0$ to $+k_0$.

Right-handed (RH) structures have limitations in space scanning. In non-periodic RH LWAs, $\beta > 0$ at all frequencies and hence, only forward angles can be obtained. In periodic RH LWAs, there are infinite number of space harmonics β_n, some of which are fast waves. The harmonics can support both backward ($\beta_n < 0$) and forward ($\beta_n > 0$) waves. However, the systematic presence of a gap at $\beta = 0$ prevents broadside radiation. A left-handed (LH) or MTM leaky wave antenna does not face the above-mentioned constraints and supports a continuous backward to forward frequency scanning. Also, since its fundamental mode is a leaky wave, no lower order guiding mode is to be suppressed and hence no complex feeding structure is needed [4].

Purely LH structures do not exist in nature since there are also RH parasitic effects. Such structures are known as composite right/left-handed (CRLH) media, whose typical transmission line (TL) model is depicted in **Figure 2(a)**. After simple manipulations, the propagation constant γ of a CRLH structure can be obtained as

$$\gamma = \alpha + j\beta = \pm j\sqrt{\left(\omega L_R - \frac{1}{\omega C_L}\right)\left(\omega C_R - \frac{1}{\omega L_L}\right)}. \tag{2}$$

http://dx.doi.org/10.5772/65643

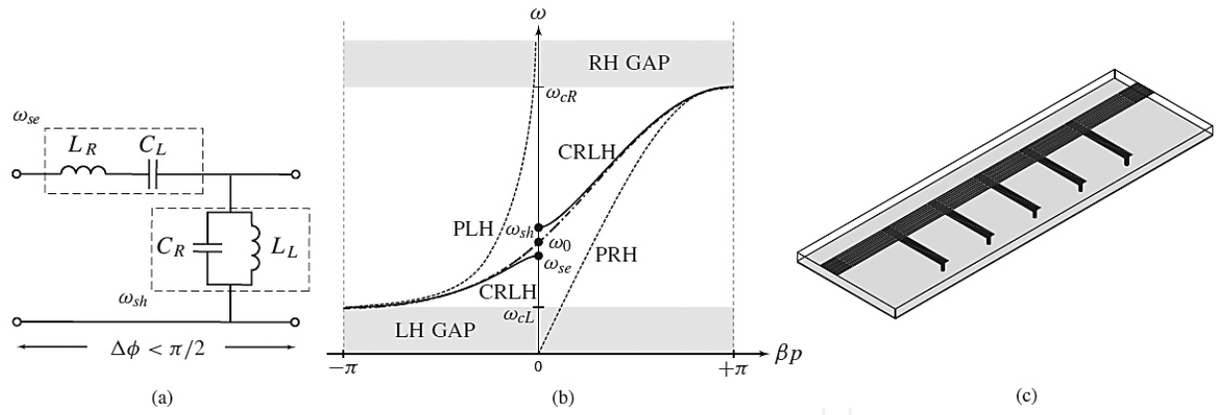

Figure 2. CRLH unit cell, (a) a typical TL model. The pairs (L_R, C_R) and (L_L, C_L) represent the RH and LH natures of the medium, respectively, (b) dispersion diagram for unbalanced case, and (c) interdigital capacitor-shunt stub implementation of CRLH unit cell [4].

Figure 2(b) shows the dispersion diagram of a CRLH unit cell. In LH and RH regions, the phase constant β is negative and positive, respectively. The frequencies ω_{se} and ω_{sh} are the through and shunt branches resonant frequencies, respectively. In a *balanced* CRLH TL, $\omega_{se} = \omega_{sh}$. In this case, the *transition* frequency ω_0 is equal to either of the resonant frequencies and there exists a broadside radiation if there is a leaky wave. In an unbalanced CRLH TL $\omega_{se} \neq \omega_{sh}$, and there exists a stop-band in this frequency range. In the dispersion diagram, the leakage radiation region ($\beta < k_0$), corresponds to inner region of a cone (radiation cone). To design a LWA the operation frequency is chosen to lie in the radiation cone. The frequencies ω_{cL} and ω_{cR} are cut-off frequencies for LH and RH regions, respectively. Note that in the stop-bands, $\beta = 0$ and from Eq. (2), $\gamma = \alpha$.

Because of their non-resonant nature, CRLH structures can be designed to exhibit simultaneously low loss and broad bandwidth. Low loss is achieved by a balanced design ($L_R C_L = L_L C_R$) of the structure and good matching to the excitation ports, whereas broad bandwidth is a direct consequence of the TL nature of the structure. Another advantage of CRLH MTMs is that they can be engineered in planar configurations, compatible with modern microwave integrated circuits [5]. A practical planar implementation of the CRLH unit cell is shown in **Figure 2(c)**. It consists of an interdigital capacitor as a series LH capacitor and a shorted shunt stub as a shunt LH inductor. Obviously, there are always parasitic RH capacitors and inductors due to the coupling between metallic trace and the ground plane. This forms a CRLH unit cell.

In the following, the most significant recent works in the context of CRLH LWAs are reviewed.

2. Electronically controlled CRLH LWA with tunable radiation angle and beamwidth [6]

Radiation angle electronic control can be explained in terms of Eq. (2). From the equivalent circuit of **Figure 2**, the dispersion diagram is obtained. Hence, from Eq. (1), the capacitors and

inductors determine the scan angle. If the one can control the capacitors by the voltage, the angle of radiation is controlled by the bias voltage, accordingly. This fact is shown in **Figure 3**.

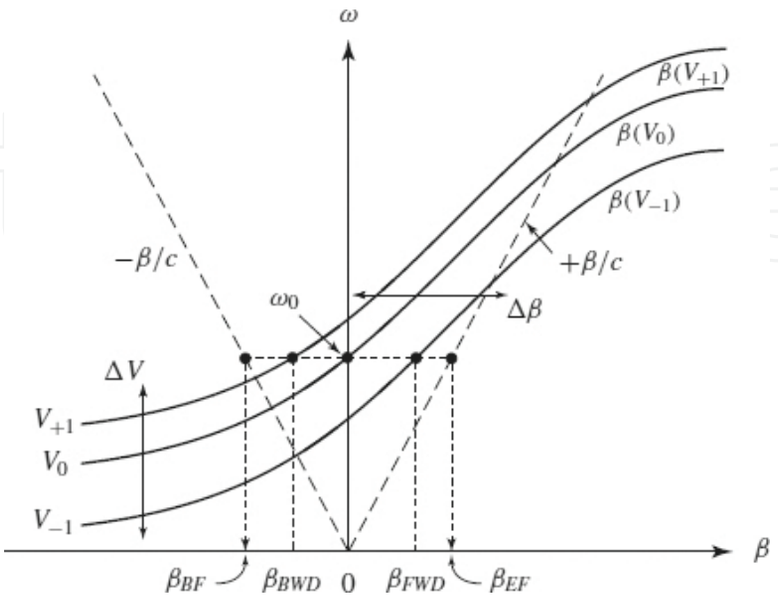

Figure 3. Principle of beam electronic scanning. Dispersion curves are shifted vertically as bias voltages are varied [6].

At a fixed frequency, the varactor diodes may control the antenna operation by a proper bias voltage tuning. The capacitance of such diodes changes by tuning the reverse bias voltage and hence, β behaves as a function of reverse bias. From **Figure 3**, by tuning the bias voltage at a fixed frequency a vertical shift happens in the dispersion diagram.

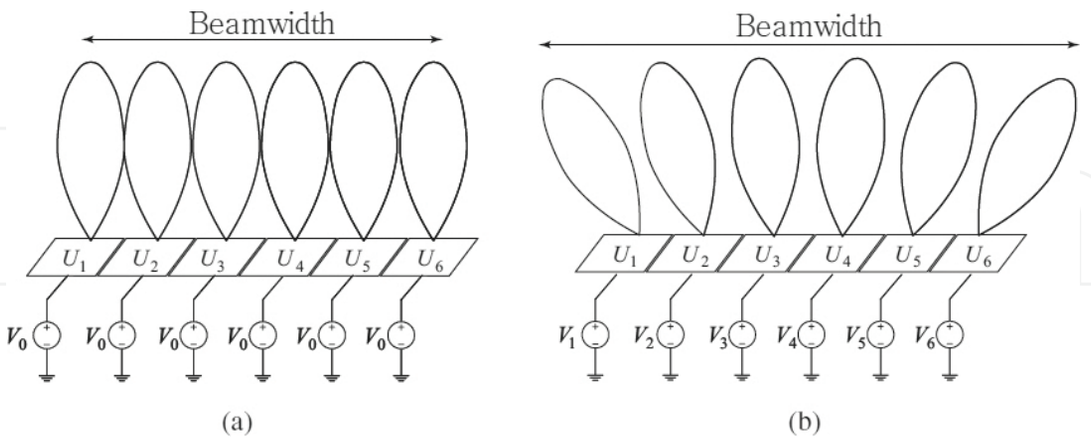

Figure 4. Principle of beamwidth electronic tuning at nonuniform biasing condition, (a) Narrow beamwidth by introduction of uniform biasing ($V_1 = V_2 = \ldots = V_0$), and (b) wide beamwidth by introduction of nonuniform biasing ($V_1 \neq V_2 \neq \ldots \neq V_0$) [6].

A uniform bias distribution along the transmission line results in a constant β and hence the LWA radiation pattern has a maximum directivity. In practice, the modification of β is difficult.

Via non-uniform biasing, the β factor of unit cells can be tuned using varactor diodes. The concept is described in **Figure 4**. When the bias distribution is uniform (**Figure 4a**), each unit cell radiates toward the same angle and the structure functions as a common LWA controlling the radiation angle. In the case of a non-uniform periodic TL, i.e., **Figure 4b**, there are different radiation angles corresponding to each cell and the beamwidth of the LWA can be controlled.

Figure 5(a) shows the layout and equivalent circuit of the voltage-controlled CRLH TL unit cell. The CRLH transmission line is loaded with varactors. One shunt and two series varactors contribute to a unit cell. A simple bias network is used to feed unit cells which, practically, can be implemented much easier than its similar counterparts. Assuming a lossless case, varactor diodes are simple modeled as a series inductor and series capacitor. **Figure 5(b)** shows the fabricated 30-cell periodic TL structure which is built on RT/Duroid5880 (ε_r = 2.2, h = 62 mil). Metelics MSV 34060-E28X Si abrupt varactor diodes are periodically distributed, and Murata chip inductors with 4.7 nH are used for dc feeds. The total length of the structure is 38.34 cm operating as a 3.3-GHz LWA. Port 1 is used for the input and Port 2 is terminated with 50 Ω in order to suppress undesired spurious beams due to mismatch reflection.

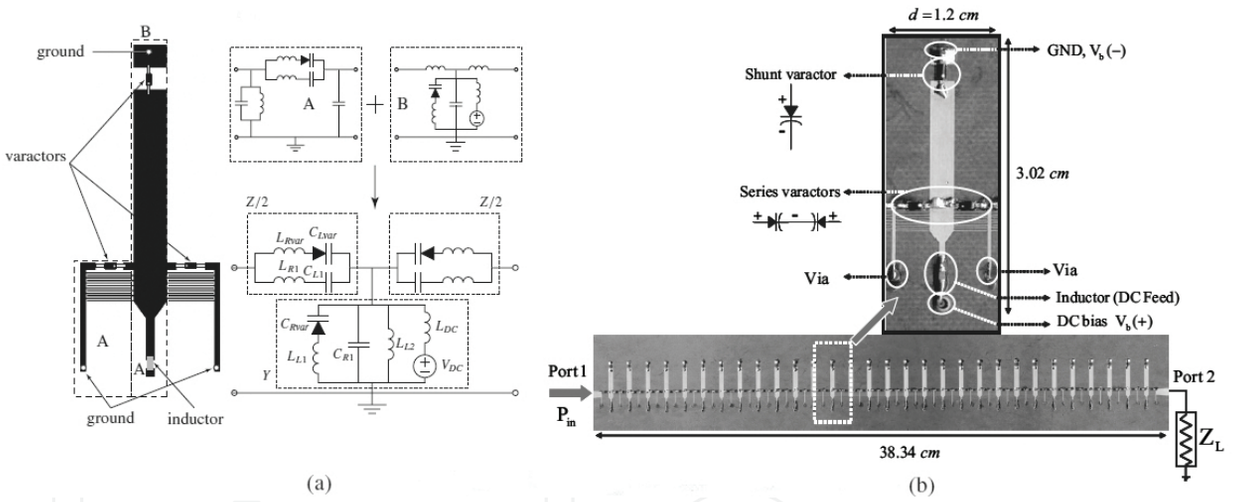

Figure 5. (a) Layout and circuit model for the varactor-loaded CRLH unit cell and (b) fabricated varactor-loaded LWA [6].

3. CRLH substrate integrated waveguide leaky-wave structure [7]

Half mode substrate integrated waveguide (HMSIW) antennas developed in [7] can support backfire to endfire radiation angle and also, its implementation is practically easy. These kinds of antennas may be fabricated by creating interdigital slots on the metal trace and ground plane of the structure. The vias and the slots perform as shunt inductor, and series capacitor, respectively. This, in turn, leads to a radiation in backward direction. The LWAs can be miniaturized by forcing them operate in the frequencies below the cutoff frequency. Also, half of the structure is utilized which makes the antenna smaller in the operating frequency.

Figure 6(a) shows the configurations of the one period CRLH SIW element. Single side and double side radiations are possible. **Figure 6(b)** shows the unit cells of CRLH HMSIW structure. For the conventional HMSIW, because of the large width-to-height ratio and the metallic via array, only the quasi-$TE_{p-0.5,0}$ ($p = 1, 2, \ldots$) modes are able to propagate in the guiding structure. In this antenna, the guided- and radiated-wave operation is fulfilled at the frequencies above and below the cutoff frequency of the waveguide. In the right unit cell demonstrated in **Figure 6(b)**, a wall constituted by metallic vias with a perfect electric conductor (PEC) strip on the wall is located. This wall is utilized to decrease the power that may leak from the boundary of the LWA. The above mentioned transmission lines can be easily mounted on the metallic surface.

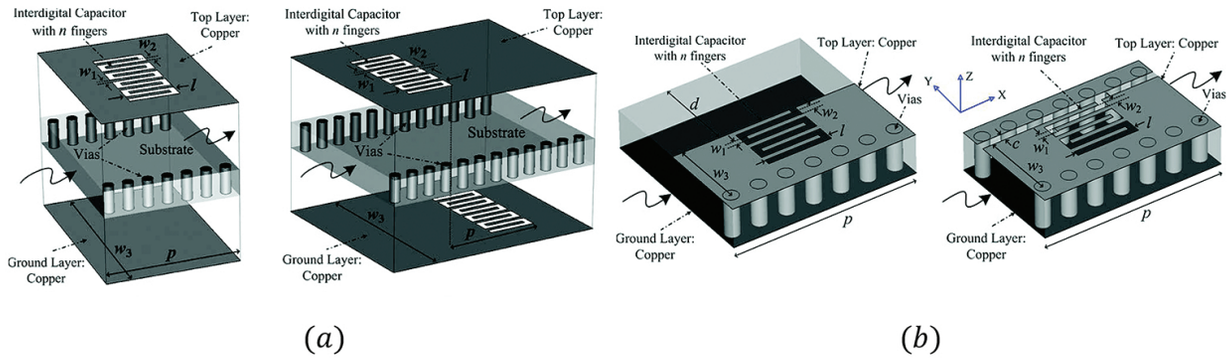

Figure 6. (a) Single side and double side radiating elements in the SIW LWA and (b) the initial unit cell and the modified folded unit cell for the CRLH HMSIW LWA [7].

Two X-band LWAs fabricated in [7] are shown in **Figure 7**. The substrate is Rogers 5880 with a thickness of 0.508 mm and relative permittivity of 2.2. **Figure 7(a)** shows one-sided and double-sided SIW LWAs. **Figure 7(b)** shows two HMSIW LWAs with unbalanced CRLH unit cells. The lower antenna is the modified folded HMSIW LWA.

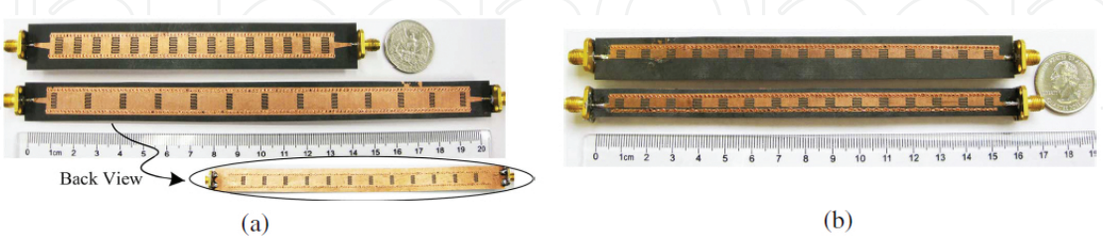

Figure 7. Fabricated LWAs, (a) SIW configuration and (b) HMSIW configuration [7].

Figure 8(a) shows the simulated and measured transmission responses of the folded HMSIW LWA. It is unbalanced and a bandgap is observed, since near the transition frequency of the CRLH unit cell the return loss is larger than its acceptable threshold.

http://dx.doi.org/10.5772/65643

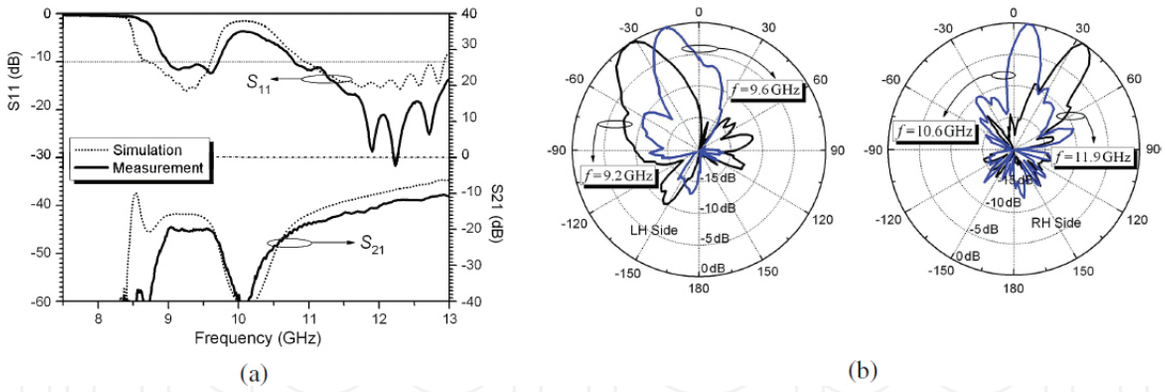

Figure 8. (a) Measured and simulated S-parameters and (b) measured E-plane radiation patterns in LH- and RH-regions, for the folded HMSIW LWA [7].

The discrepancy between the measurement and simulation is due to the fact that the conductor loss and dielectric loss in the measurement should be higher than that in the simulation. By changing the slot size and the position of the vias the position of the LH band can be controlled. Balanced condition can also be obtained by some optimizations. **Figure 8(b)** shows the E-plane radiation patterns for the folded CRLH HMSIW LWA. Beam frequency-scanning capability in E-plane is clearly observed. Since this is an unbalanced case and there is no balanced point which gives broadside radiation it is difficult to obtain the H-plane patterns. The edge radiation in HMSIW LWA is slightly higher compared with the SIW LWA, which is mainly due to edge radiation caused by the open boundary.

4. High gain active CRLH LWA [8]

In the reference [8], a high-gain CRLH LWA is presented to operate at broadside. It is constituted by passive CRLH leaky-wave sections interconnected by amplifiers, which regenerate

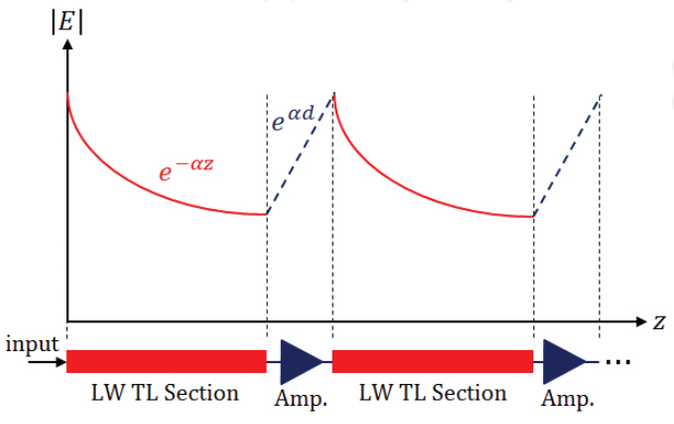

Figure 9. In an active LWA, the field intensity (exponential) loss is compensated by amplification [8].

the power progressively leaked out of the structure to increase the effective aperture of the antenna and thereby its gain. The gain is further enhanced by a matching regeneration effect induced by the quasi-unilateral nature of the amplifiers. The principle of gain enhancement is shown in **Figure 9**.

Practically, a matched load is located at the end of the leaky-wave antennas. The power has leaked by 90% before reaching the termination point since no more increase in the radiation area of the antenna is no more achieved. On the other hand, if the guided wave is boosted periodically, the gain of the LWA can be arbitrarily increased. Another advantage is that this provides with the new possibility of achieving arbitrary current distributions along the antenna metallization and henceforth generating arbitrary radiation patterns. The fabricated active LWA is shown in **Figure 10(a)**. As shown in **Figure 10(b)**, the amplifier is on the bottom layer and is connected to the top microstrip line through vertical transition of vias. The amplification loop is designed to provide a zero phase shift from its input to its output in order to play a neutral role in terms of phase at the transition frequency ($\beta = 0$).

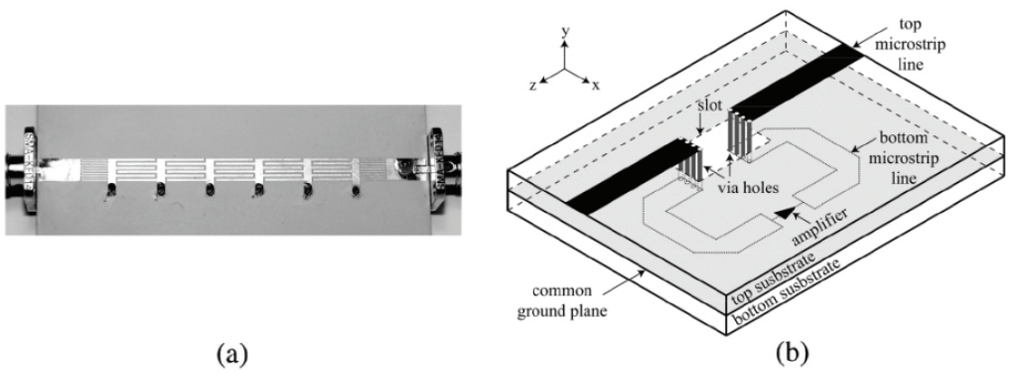

Figure 10. (a) The fabricated active LWA and (b) microstrip-to-microstrip vertical double transition to embed the amplifier in the unit cell [8].

5. Reflecto-directive system using CRLH LWA and heterodyne mixing [9]

In the reference [9] a system receives a signal at a fixed frequency with a patch antenna and reflects it back toward any desired angle by tuning the LO frequency of a mixer. The principle of operation is based on the reception of a wave at a fixed frequency by a quasi-omnidirectional microstrip receiver and retransmission of it to an arbitrary direction by a full space scanning LWA. One can accomplish the new function by way of heterodyne mixing. A schematic of the reflecto-directive system is shown in **Figure 11(a)**. In this schematic, two mixers are required if f_{in} lies in the band of the LWA. In the case of utilizing only one mixer, the incoming wave cannot be filtered and hence it contributes to generation of an undesired angle existing at the input frequency. The mentioned fact is practically cause trouble to the reflecto-directive system and is maintained using a circuit including two mixers, where the signal at the input frequency is removed using a low-pass filter placed just before the second mixer. The reflecto-directive system prototype is shown in **Figure 11(b)**.

http://dx.doi.org/10.5772/65643

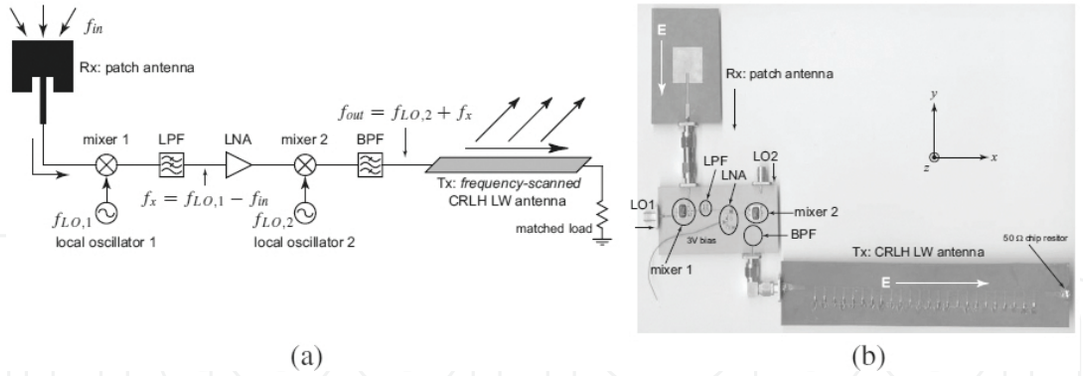

Figure 11. The reflecto-directive system, (a) schematic and (b) prototype. The polarization of RX and TX antennas are along *y*-direction [9].

The source test antenna sends a signal at the frequency of 5 GHz at two different fixed angles $\theta_{in} = -30°, 30°$ .The radar cross section of the reflecto-directive system is measured in the frequencies, $f_{\text{out}} = 3.5$ GHz, 4.5 GHz and 5.5 GHz. Based on the following relation, the corresponding $f_{LO,2}$ for each input frequency can be obtained.

$$f_{LO,2} = f_{out} + f_{in} - f_{LO,1}. \tag{3}$$

The results are shown in **Figure 12**. For all the incidence angles tested, clear radar cross section (RCS) peaks appear at the angles −20°, +20°, and +50° for the frequencies f_{out} = 3.5 GHz, 4.5 GHz and 5.5 GHz, respectively, in agreement with the LWA angle-frequency relation.

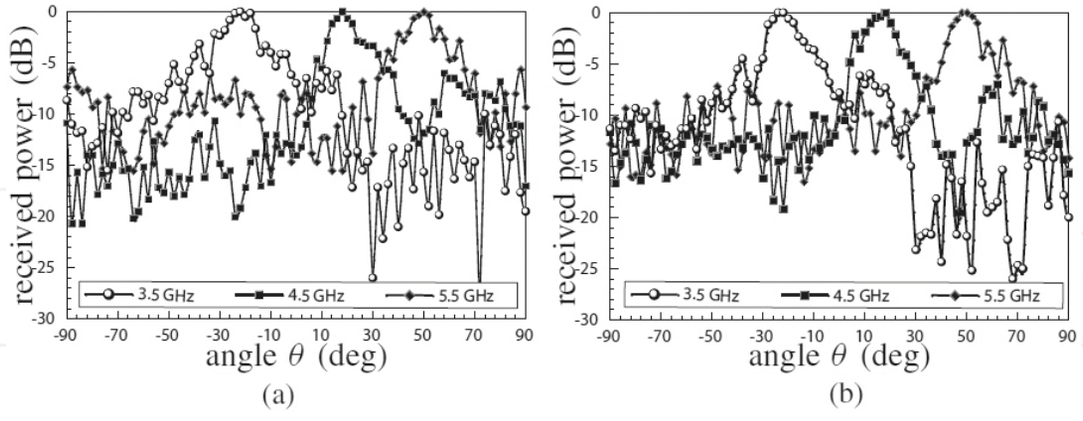

Figure 12. Measured bistatic RCS of the reflecto-directive system [9].

6. Dual band LWA on a CRLH substrate integrated waveguide [10]

The idea of the antenna design in [10] is based on dual band/quad band operation of the CRLH TL. The layout of the proposed dual band SIW LWA in [10] is shown in **Figure 13**. In its unit

cell equivalent circuit, the series elements are represented mainly by the meander slots that enable the antenna to radiate, and the parallel elements are represented by four conducting vias.

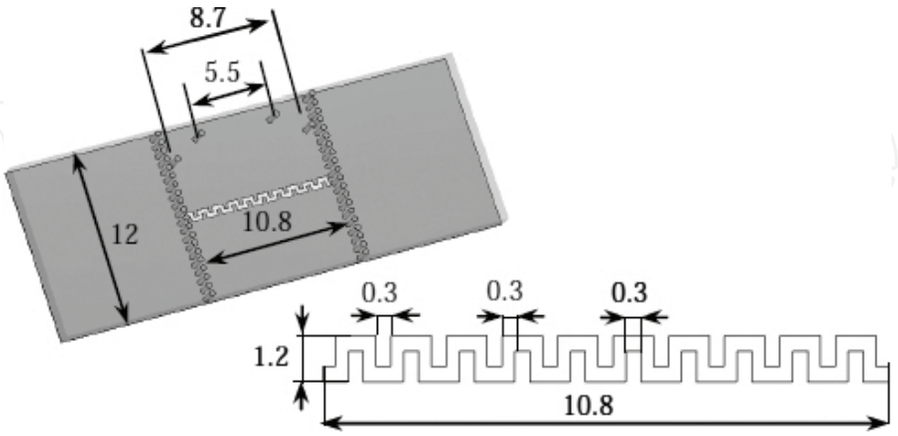

Figure 13. Layout of the meander slot and the SIW unit cell setup [10].

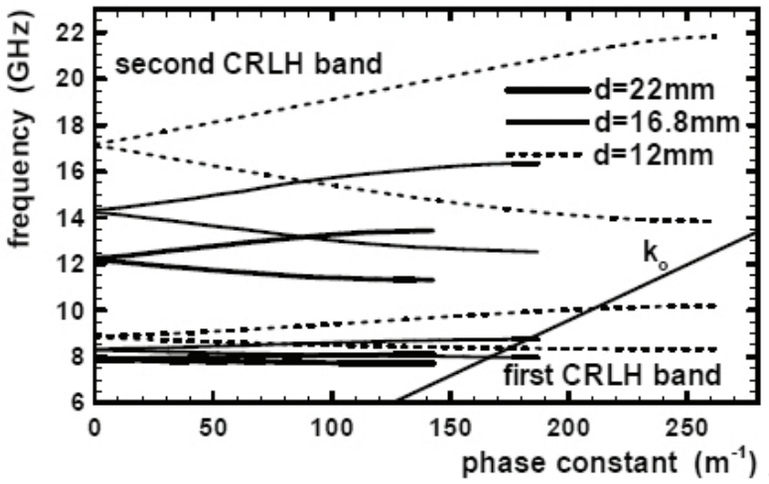

Figure 14. Dispersion diagram of the dual-band LWA for different cell lengths. The three antennas also differ in SIW width [10].

An undesired radiation exists in the antenna since in the structure when the relation $\beta d = \pi$ is satisfied, the Bragg phenomenon takes place. Bragg reflection occurs when the dispersion diagram is at its edges. The dispersion diagrams of the antennas are demonstrated in **Figure 14**. The unit cell lengths in these antennas are different. **Figure 14** shows that the central frequency of the higher frequency band is controlled mainly by the length of the unit cell and the central frequency of the lower band is mainly determined by the SIW width. If $\beta d = \pi$, spurious radiation occurs. This can be removed by shifting this point into a non-radiating area, or at least to the close proximity of it. The drawback is of course that the steering beam span is reduced. From **Figure 14**, the antenna dual band operation is clearly observed. A photograph

of the 25-cell antenna is shown in **Figure 15**.A quarter-wavelength transformer was used to transform the real part of Z_{in} to nearly the same value as the impedance of the empty SIW. The transformer is located at the point where the imaginary part of Z_{in} is almost equal to zero. The main advantage of this type of matching is that it matches the first band of the antenna, but it simultaneously does not affect the second band.

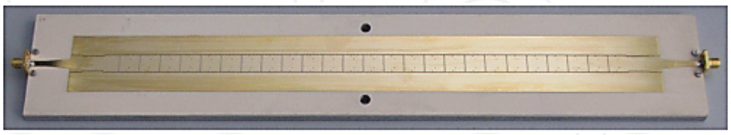

Figure 15. The fabricated dual-band SIW LWA [10].

The measured radiation patterns of the antenna in the longitudinal plane normal to the antenna are shown in **Figure 16**. Part (a) and (b) of **Figure 16** correspond to lower- and higher-frequency bands of the antenna, respectively. Steering the direction of the main lobe from backward to forward by changing frequency in the two frequency bands is obvious. In the second band, the pencil beam is narrower but the beam steering is less sensitive as the beam spans a smaller angular range.

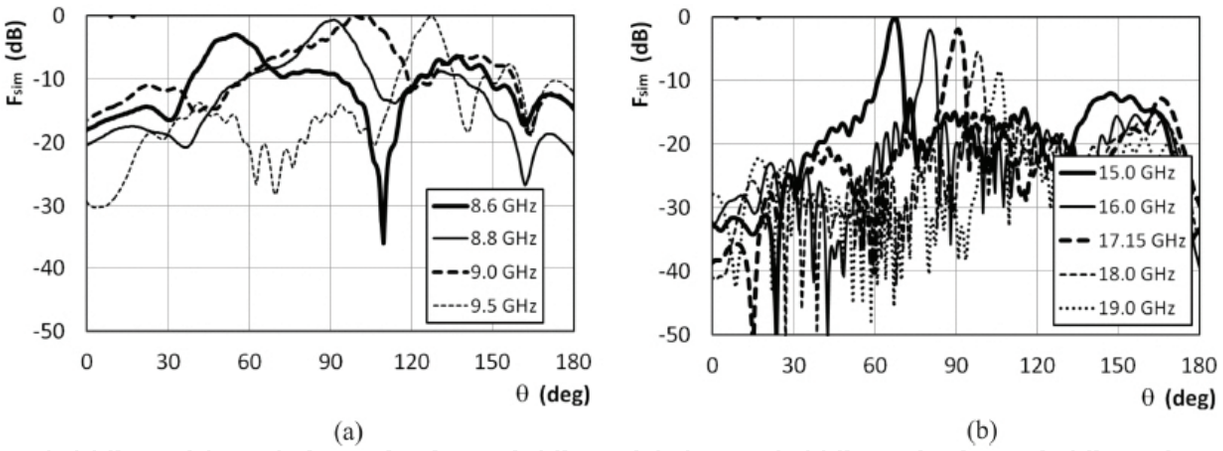

Figure 16. Measured radiation patterns, (a) first band and (b) second band [10].

7. Dual band full space scanning LWA based on ferrite loaded waveguide [11]

The ferrite-loaded open structure is shown in **Figure 17(a)**. It is a waveguide fully filled with ferrite with one side wall removed and magnetized by the bias field H_0. At the frequency band in which n_e is much larger than one ($n_e \gg 1$), the side wall of the structure which is the interface between vacuum and magnetized ferrite, can be assumed as a perfect magnetic conductor (PMC) medium.

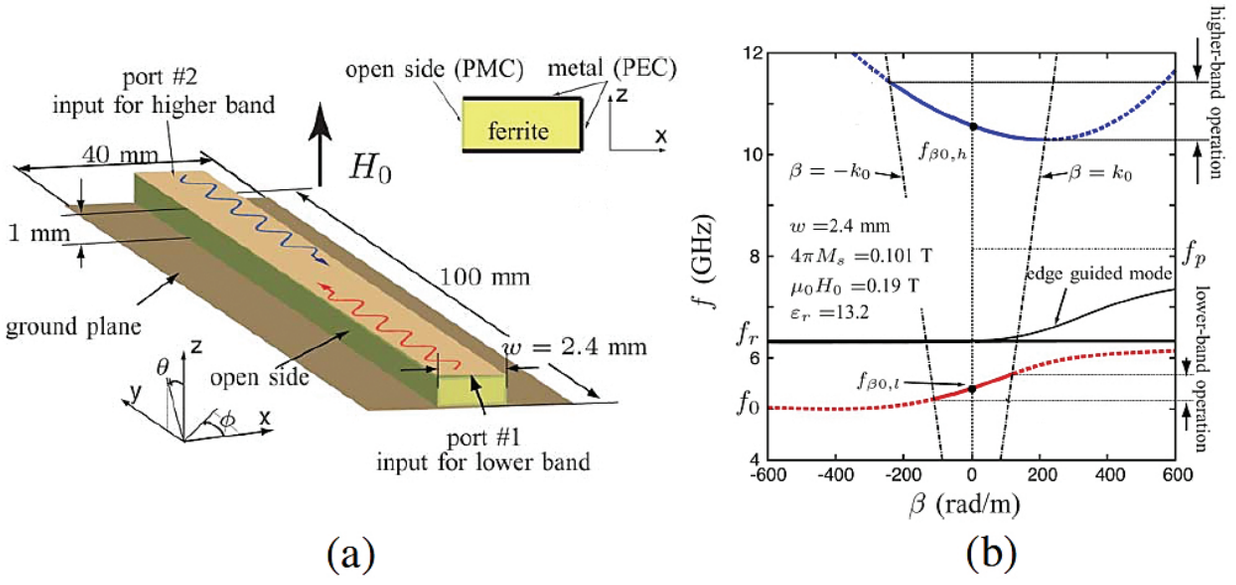

Figure 17. (a) Ferrite-loaded open waveguide structure and (b) its dispersion diagram [11].

The dispersion relation of the structure in **Figure 17(b)** is

$$\tan\left(k_x w\right) = -\frac{\mu k_x}{\beta \kappa}, \tag{4}$$

with $k_x = \sqrt{\omega^2 \varepsilon \mu_e - \beta^2}$, and μ and κ are the elements of Polder tensor permeability, and μ_e is the effective birefringent permeability of the structure, corresponding to a bias field H_0 perpendicular to the direction of propagation β. The dispersion diagram computed by Eq. (4) is shown in **Figure 17(b)**. Essentially, three bands may be observed in the frequency range shown. The lower band is the CRLH mode, the second band is the edge-mode band, and the higher band is called mixed forward/backward perturbed TE_{10} mode. In this LWA only the leaky modes are of interest. These modes are present at the lowest and the highest bands.

From $v_g = d\omega/d\beta$, the lower band CRLH leaky mode exhibits a positive group velocity v_g at all frequencies. Since $v_g > 0$, power flows in the positive y-direction. In contrast, due to non-reciprocity of the structure and the subsequent nonexistence of a $v_g < 0$ mode, no energy can propagate toward the source in this mode, even in the case of reflection, where power would be dissipated in heat instead of propagating. The phase velocity of the lower-band CRLH mode changes sign from negative to positive at the transition frequency when frequency is increased. From the scanning law for the main leaky-wave beam, the structure exhibits full-space radiation from backfire to endfire. The higher band leaky mode exhibits a negative group velocity at the frequencies within the leaky-wave region, which is the region of interest. The phase velocity of the higher perturbed waveguide mode is negative and positive below and above the transition frequency leading to full space beam scanning.

http://dx.doi.org/10.5772/65643

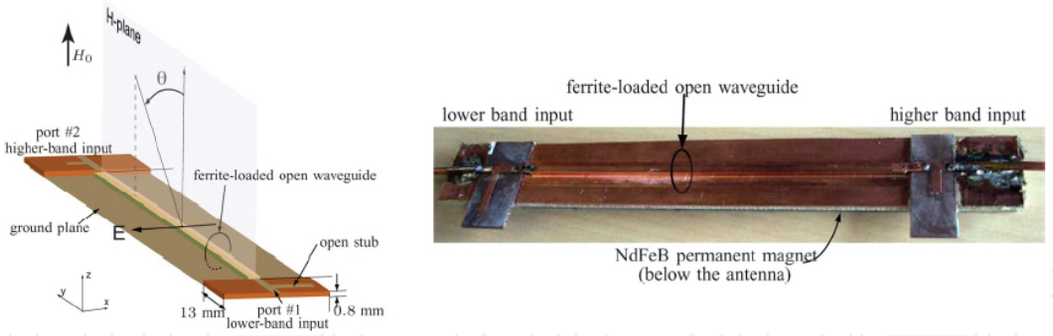

Figure 18. The configuration and prototype of the ferrite-loaded open waveguide [11].

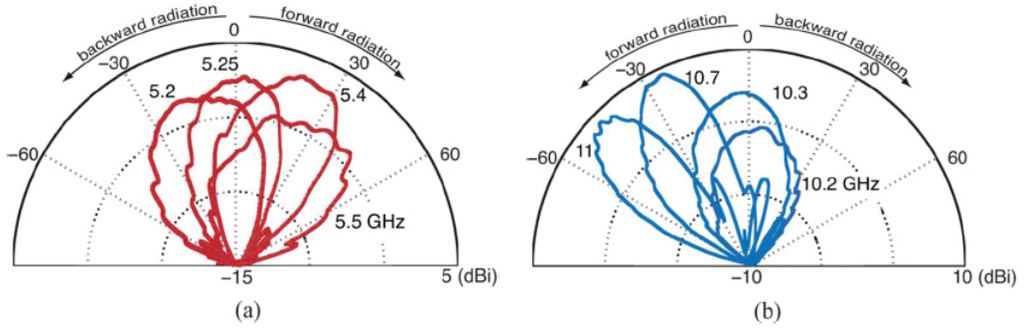

Figure 19. Measured frequency beam scanning, (a) lower band and (b) higher band [11].

Figure 18 shows the configuration and the prototype of the dual band antenna with microstrip-to-waveguide transitions and lower-band/higher-band stub matching sections at both ends of the structure. The measured radiation patterns are shown in **Figure 19**. Note that due to the fact that the ports of the two modes are placed at the opposite ends, the forward and backward spaces are reversed between the two modes.

8. Fundamental-mode LWA using slot-line and split-ring-resonator (SRR)-based MTMs [12]

The key point in [12] in the fact if the slots in a coplanar waveguide (CPW) TL have a relatively far distance from each other, the structure is regarded as two independent TLs loaded with slots both lying on a dielectric substrate, which have two magnetic currents with 180 ° phase shift. The propagation characteristics of the CRLH CPW TL based on split-ring-resonators (SRRs) and wires can be obtained through the analysis of the dispersion relation. This can be inferred from the lumped element equivalent circuit model of **Figure 20(a)**. The implementation of the CRLH slotline LWA is shown in **Figure 20(b)**. The antenna is essentially a host slotline periodically loaded with SRRs and narrow metallic strips. The unit cell was obtained by removing one of the halves of the CPW unit cell. The loaded line is matched to a connector

using a semi-lumped microstrip-to-slotline transition acting as an inductive transformer-based matching network.

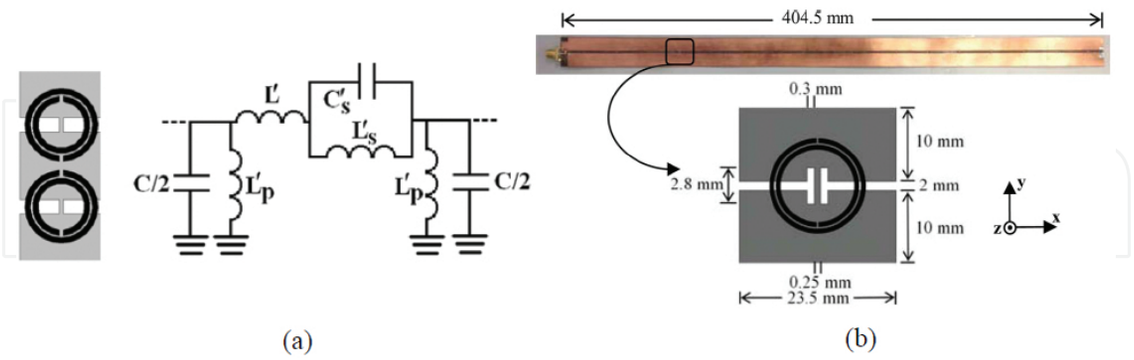

Figure 20. (a) Layout of the unit cell of the CPW structure with SRRs (etched in the back substrate side) and its simplified equivalent circuit and (b) fabricated LWA [12].

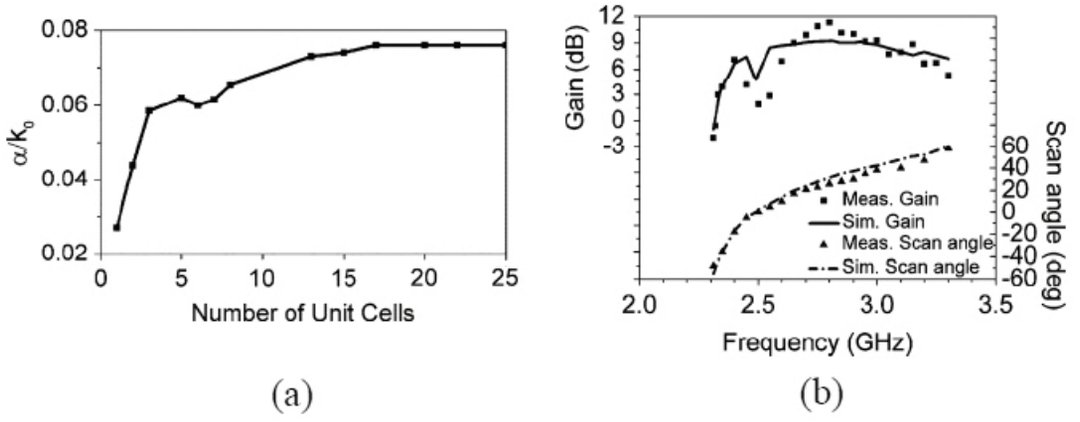

Figure 21. The SRR-based LWA, (a) attenuation constant versus the number of unit cells at 2.5 GHz and (b) gain and scan angle [12].

Because of edge effects and mutual coupling, the attenuation constant (α)of an LWA cannot be obtained through the analysis of a unit cell. In this case, if the number of cells increases, one can neglect the edge effects and calculation of α become more accurate. Demonstrated in **Figure 21(a)** is α/k_0 which is normalized to the free space wavenumber. As seen, at least 15 unit cells are needed to reach the value $\alpha/k_0 = 0.076$. The obtained attenuation constant is utilized to derive the length of leaky wave antenna using relation Eq. (5) as stated below:

$$P_n = P_0 e^{-2\alpha nd}, \tag{5}$$

where d is the periodicity, P_0 is the power delivered to the LWA and P_n is the power at the nth terminal. For 95% of the power dissipated before reaching the antenna termination and using the converged value of $\alpha/k_0 = 0.076$, the needed number of unit cells is obtained to be $N = 17$.

http://dx.doi.org/10.5772/65643

Figure 21(b) shows the measured and simulated LWA gains. For the LH and RH frequency bands, the maximum measured gains are respectively 7.1 and 11.3 dB. Since the LWA balance condition at the transition frequency is not satisfied, the gain reduces at broadside angle. This results in a quite wide main beam at broadside. The existence of an evanescent mode at 2.5 GHz makes shorter the effective aperture length of the LWA and hence imperfect matching at broadside. The main beam angle as a function of frequency is also plotted in **Figure 21(b)**. The backward to forward scanning ranges from − 50 ° to + 60 ° while maintaining an acceptable gain level.

9. Conformal CRLH LWA [13]

In the reference [13], a conformal mapping-based method to analyze and synthesize singly-curved microstrip structures is reported. Conformal mapping is a powerful method which has been applied to study the guided- and radiated-wave characteristics of microstrip patch antennas [14–16]. Also, it is applied to CRLH LWAs in [13, 17]. The cross-section of a singly-curved surface is usually an elongated region with curved boundaries, as shown in **Figure 22(a)**.

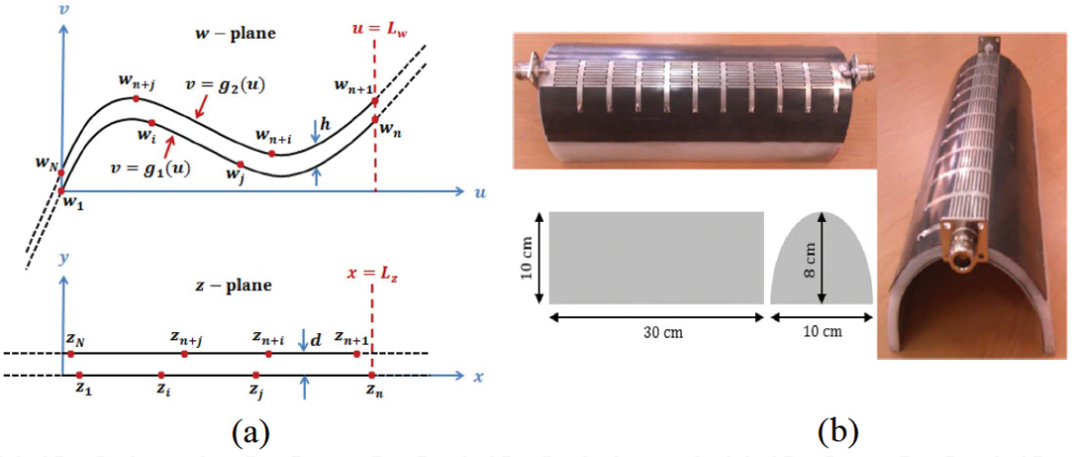

Figure 22. (a) Curved strip and the infinite straight strip mapped to the curve and (b) fabricated conformal CRLH LWA [13].

An elongated polygon may be mapped through the Schwartz-Christoffel transformation (SCT) to a new finite polygon. However, this may result in an undesirable effect called crowding. In order not to let the crowding effect take place, the transformation is adapted to map a long and straight strip to an infinite polygon. This polygon must have two ends at infinity. This is shown in **Figure 22(a)**. Curvature is accounted for by fitting each segment of the curved boundaries with a second degree polynomial function of SCT prevertices. This mapping is called modified Schwarz-Christoffel transformation (MSCT).

In some applications the utilization of conformal antennas is inevitable. For example on a vehicles' body if the antenna does not completely stick to the surface, it causes trouble in

aerodynamics point of view. Hence, a conformal antenna which also makes the vehicle less visible, is installed on the body. In the reference [13], the MSCT approach is used to design a CRLH LWA on an elliptic surface, as shown in **Figure 22(b)**. The dispersion diagram and Bloch Impedance of a unit cell of the antenna are shown in **Figure 23**, which show good agreement between the MSCT method and full wave simulation (CST commercial package). Bloch impedance is a counterpart to characteristic impedance in periodic TLs. Also, the theoretical results predicted the measurements of the CRLH LWA.

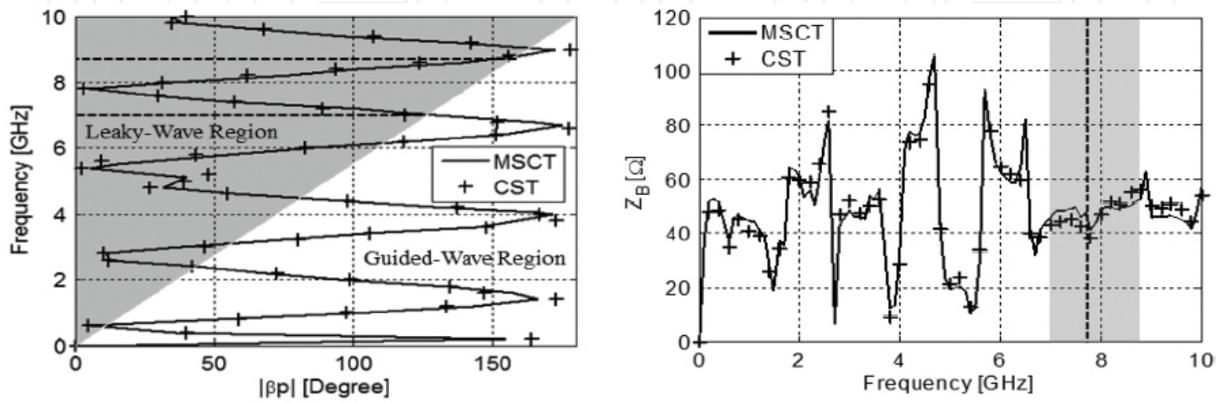

Figure 23. The dispersion diagram and Bloch impedance of the elliptic CRLH LWA unit cell. The shaded region is attributed to the leakage radiation frequency band [13].

10. Broadband CRLH LWA designed on dual-layer SIW [18]

In the reference [18], a dual-layer SIW X-band LWA with a bandwidth of 66 % beside 105° of the beam steering angle is obtained both in RH and LH regions. The top and side views of the wideband antenna are shown in **Figure 24**. The radiation aperture is provided by the interdi-

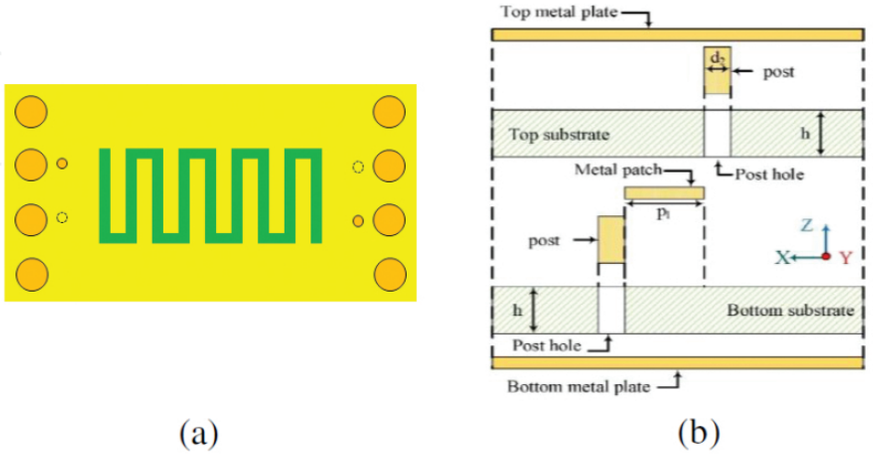

Figure 24. The designed dual-layer SIW antenna, (a) top view and (b) side view [18].

http://dx.doi.org/10.5772/65643

gital capacitor slots, as shown in **Figure 24(a)**. Increasing the total inductance of the structure is a way to tackle the existence of band gap at the operational bandwidth of the antenna. In this way the balanced conditions will be satisfied in a higher frequency, so the LH region will be extended. Using inductive elements to increase the inductance of the structure much more than what is provided by the nature of waveguide, is obtained with a twisted post which is realized by two metallic vias in the top and bottom substrates and are connected to each other using a metal patch etched on the top surface of the bottom substrate. **Figure 24(b)** illustrates the metallic posts and the metal patch in order to obtain the twisted post. The side wall vias of the SIW are not shown.

The dispersion diagram of the proposed unit cell in [18] is depicted in **Figure 25(a)**. The balanced condition is satisfied at 6.8 GHz. A wide frequency band attributes to the radiating region in both LH and RH bands which yields a wideband LWA. The scattering parameters of the LWA consisting of 10 unit cells are depicted in **Figure 25(b)**. S_{11} is less than − 10 dB and S_{21} is kept below −3 dB, which is suitable for operating the LWA. The antenna provides a fractional bandwidth of 66%.

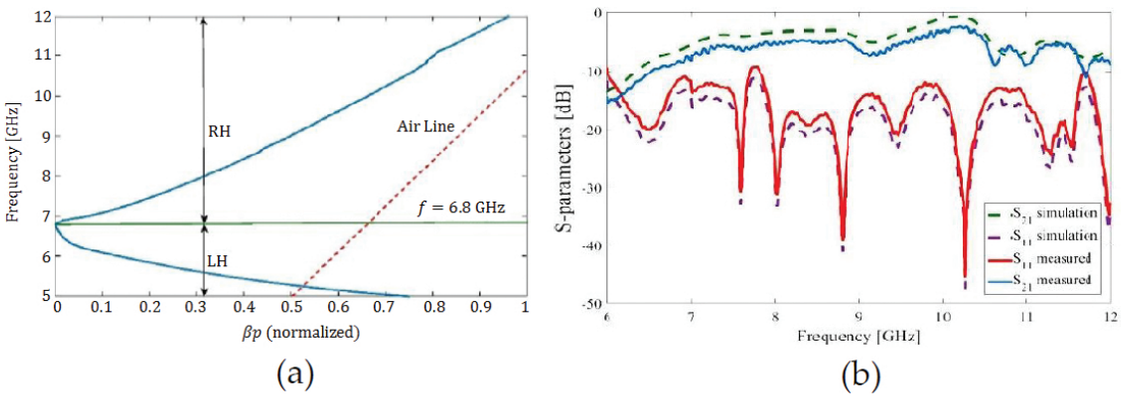

Figure 25. (a) Dispersion diagram of the unit cell and (b) scattering parameters of the 10-cell LWA [18].

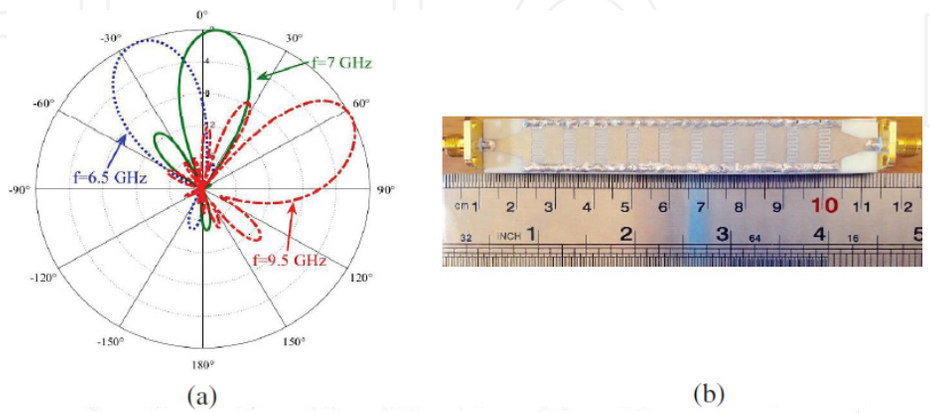

Figure 26. (a) The radiation patterns and frequency scanning of the beam and (b) the fabricated wideband dual-layer SIW LWA [18].

The radiation patterns of the X-band antenna with the property of beam sweeping are shown in **Figure 26(a)**. The LWA can change the direction of main lobe from −34° up to +72° including the broadside. There is a tradeoff between the bandwidth and the gain of the antenna. The sensitivity of gain, side-lobe level (SLL) and half-power beamwidth (HPBW) of the antenna in [18] is low and this is an important feature.

The fabricated antenna with the total dimensions of 100.2 mm × 13.53 mm × 1.69 mm is shown in **Figure 26(b)**. A wide variety of techniques are available to feed SIW structures, one of them is the tapering transition from microstrip to SIW, which is used in [18] to feed the LWA.

11. Single radiator CRLH circularly polarized LWA [19]

In the reference [19], a compact SIW CRLH-loaded LWA is proposed. The main advantage of the antenna is its pure circular polarization and also its compact size. A schematic of the unit cell is demonstrated in **Figure 27(a)**. Two interdigital slots are embedded in a single cell. The sections 2 and 3 each make 90° phase difference. The interdigital slots have angular separations of +45° and −45° with respect to the direction of wave propagating in the waveguide. This generates a circularly-polarized leaky wave radiation. As shown in **Figure 27(a)**, two microstrip lines are added to the cell in sections 1 and 4, with each section making 90° phase shift. This introduces a total phase shift of 360° to the unit cell. Hence, all the unit cells in the LWA have in-phase radiation and the constructive effect improves the directivity of the LWA.

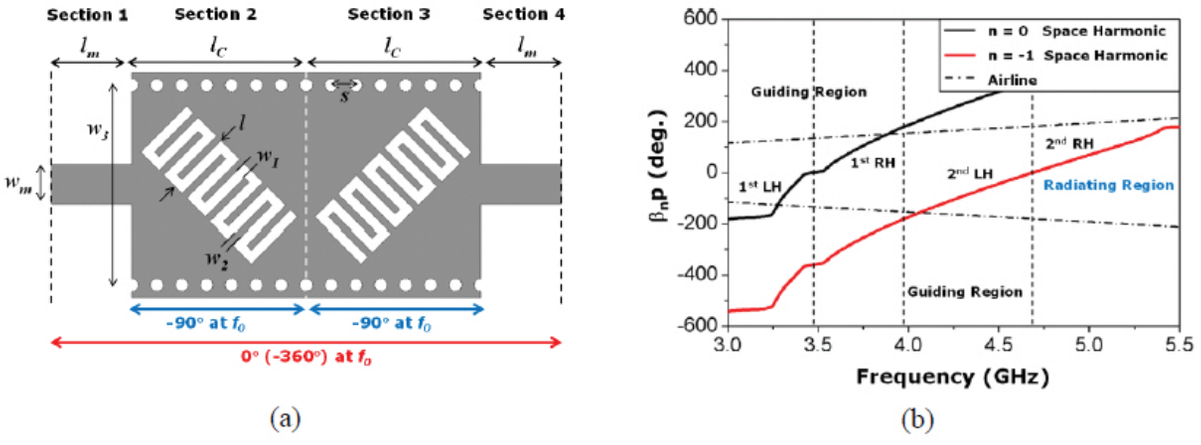

Figure 27. SIW circularly polarized CRLH LWA, (a) unit cell and (b) dispersion diagram [19].

The microstrip lines play the role of a matching circuit and this prohibits the use of an external matching network which leads to a compact antenna. Also, the placement of the two slots needs only one feed and hence there is no need to use a quadrature hybrid coupler to introduce a circular polarization. Therefore the antenna is a single radiator LWA. **Figure 27(b)** shows the dispersion diagram for the harmonics $n = 0$ and $n = -1$ which is clearly a multiband operation. The balanced conditions are also satisfied leading to the possibility of broadside radiation.

http://dx.doi.org/10.5772/65643

Figure 28(a) demonstrates the fabricated antenna and **Figure 28(b)** shows the LWA axial ratio clearly illustrating its relatively pure circular polarization. The application of circular polarization is inevitable in harsh environments. As an example a satellite moves dynamically and it is not possible to align the receivers (such as GPS system) to the satellite. Hence in this case the circular polarization is used instead of linear polarization.

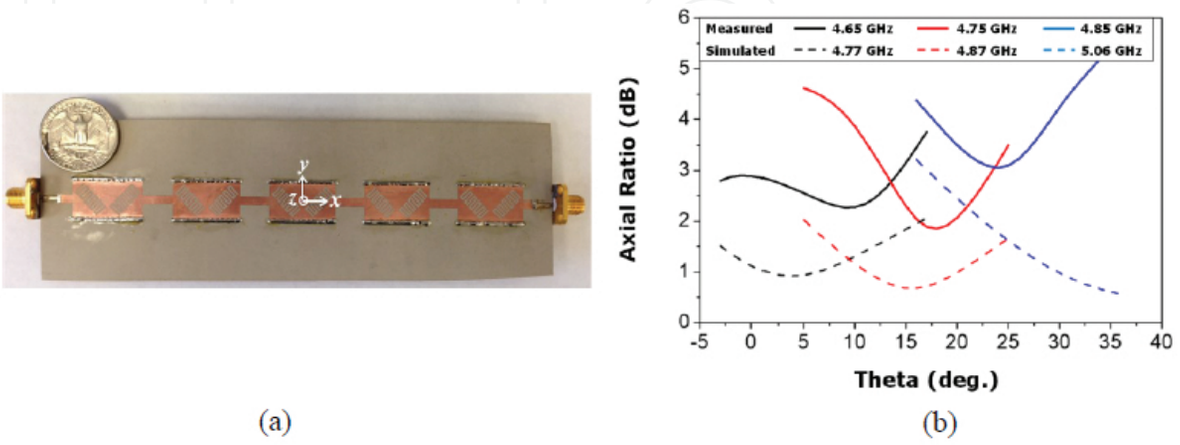

Figure 28. (a) The fabricated single radiator LWA and (b) the axial ratio diagram representing circular polarization [19].

12. Non-cutoff SIW-based LWAs [20]

In the reference [20] a SIW LWA is proposed which is based on a waveguide operating above its cutoff frequency. Note that in many conventional LWAs, the leaky wave radiation is based on below-cutoff guiding operation. A schematic of the proposed unit cells in [20] is demonstrated in **Figure 29**, where the left and right cells pertain to initial and modified unit cells. In the initial cell design in **Figure 29(a)**, the transverse slot can be modeled by a series impedance and the longitudinal slot is modeled by a shunt admittance. The field distribution in the transverse slot is minimum at its center and is maximum at its ends, hence it behaves like an inductor in the transition frequency. In the longitudinal slot, the field distribution is reversed and hence it plays the role of a capacitor. At the transition frequency, one can easily satisfy the condition $S_{11} = 0$ and therefore the open stopband can be suppressed. This results in a seamless broadside radiation.

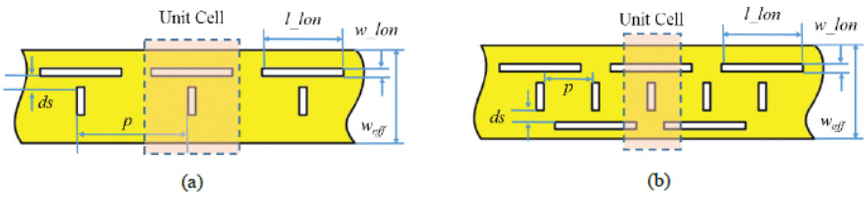

Figure 29. The unit cells for above-cutoff operation and suppression of open stopband in a LWA, (a) initial cell and (b) modified cell [20].

The scattering parameters for the simulated LWA are shown in **Figure 30(a)**. The transition frequency is 11.8 GHz and hence as shown in Figure REF fig30 \ h 30, the antenna can radiate in backward and forward angles. There is a peak in S_{11} at the transition frequency and this shows that even though the open stopband is suppressed, the effect of spurious reflections is observed. **Figure 30(b)** shows the main lobe direction and realized gain for the simulated antenna. The antenna supports scanning angles between −70° and 30°. The maximum realized gain happens at forward angles and is about 70 dB.

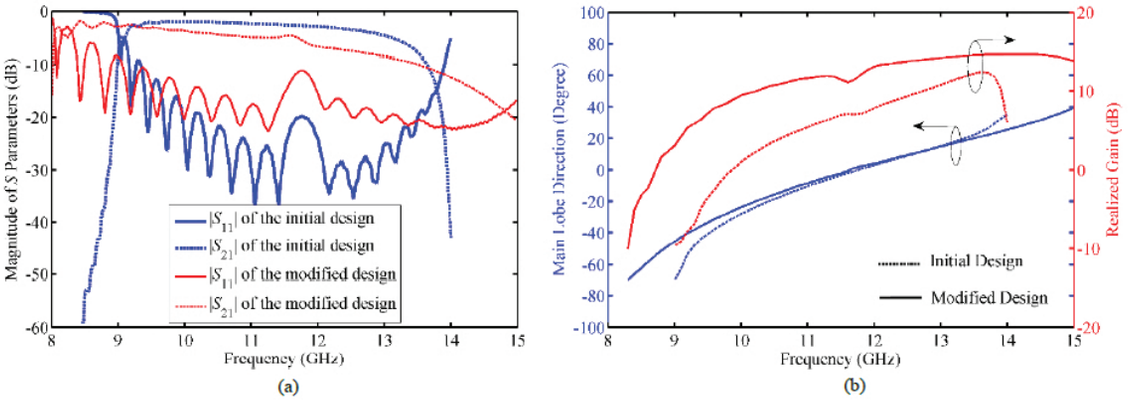

Figure 30. (a) Scattering parameters and (b) main lobe direction and realized gain [20].

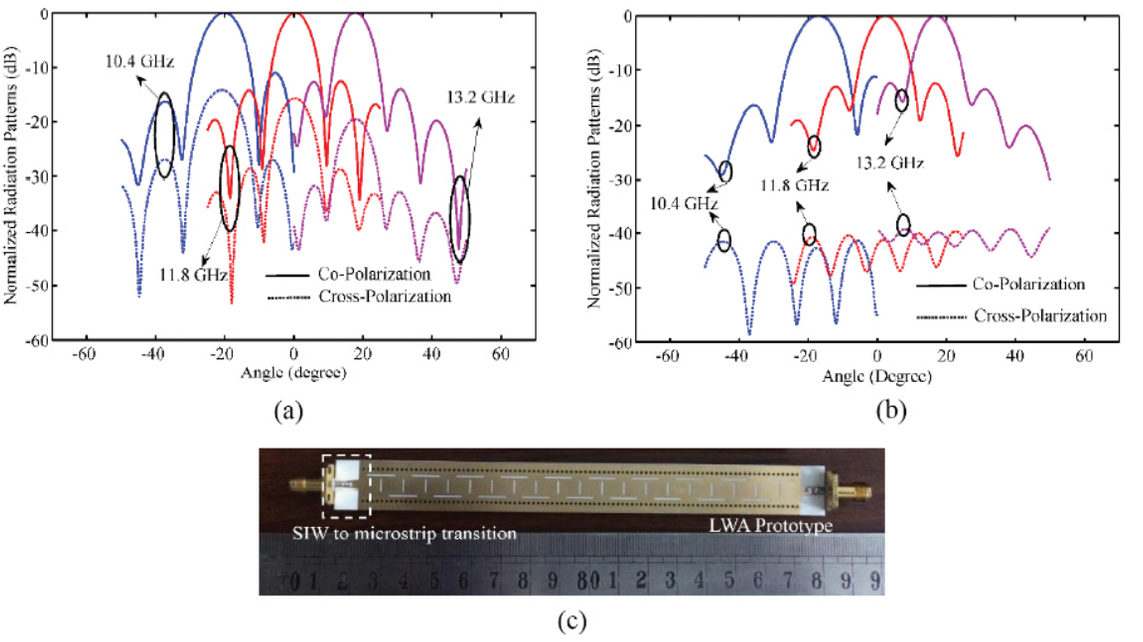

Figure 31. Backward, broadside and forward radiation patterns for the LWA comprising (a) initial unit cells and (b) modified unit cells. (c) The fabricated LWA using modified cells [20].

The radiation patterns for backward, broadside and forward angles for co- and cross-polarizations in the LWA with initial unit cells are shown in **Figure 31(a)**. The frequency scanning of

the beam is clearly observed. When using the modified unit cell of **Figure 29(b)**, the antenna become more compact, since the condition of in-phase radiation for the cells is satisfied for a smaller unit cell. Also, as shown in **Figure 30(a)** it has a more efficient behavior in scattering parameters. It renders S_{11} below −10 dB and concurrently, reduces the insertion loss resulting in increasing the leakage rate. Accordingly, the realized gain is improved, as demonstrated in **Figure 30(b)**. Also, its gain is more flat compared to the initial unit cell. **Figure 31(b)** shows that the modified unit cell results in lower cross-polarization compared to **Figure 31(a)**. The fabricated antenna including modified unit cell is shown in **Figure 31(c)**.

13. Programmable LWA with J-shaped MTM patches [21]

Reference [21] has introduced a novel J-shaped unit cell which has the ability of digital tuning of the beam at a fixed frequency. This can be a potential alternative to complicated phased arrays. A schematic of the antenna with its unit cell is shown in **Figure 32(a)**. The J-shaped patch is a CRLH cell, since the shunt inductor is formed by the virtual ground at the top of the patch. Other circuit equivalents are clearly deduced. In each unit cell, the upper gap can be open (ON) or close (OFF). This is the base for digital tuning and is demonstrated in **Figure 32(b)**.

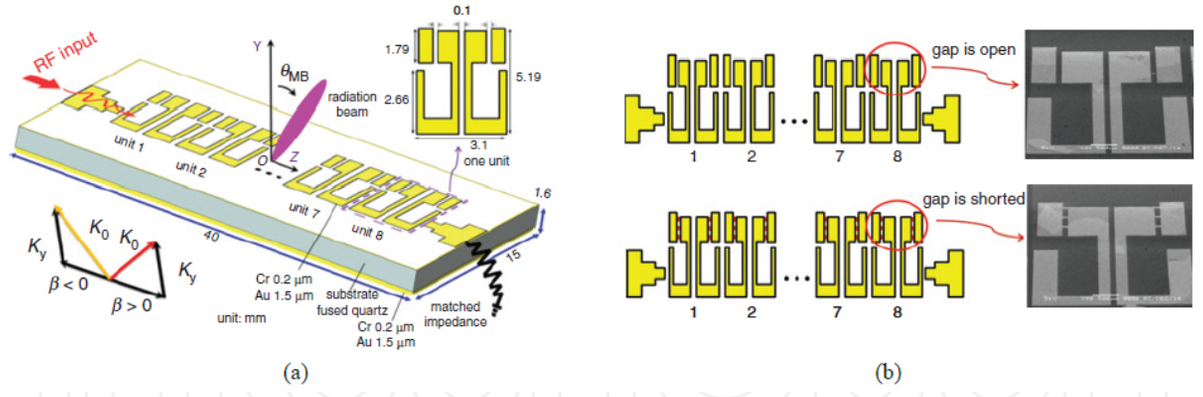

Figure 32. (a) Programmable LWA and its J-shaped patch unit cell and (b) the ON and OFF states in the J-shaped patch [21].

In a LWA with N unit cells, 2^N different digital states can be programmed. In the reference [21] a LWA with eight elements is considered and then 256 states are possible. Among the states, nine samples including different ON-OFF states are studied. Since at a fixed frequency, changing each state changes the propagation constant of the LWA, it also changes the main beam direction. **Figure 33(a)** shows the realized micromachined LWA and **Figure 33(b)** illustrates the beam scanning with digital states. The left and right patterns pertain to simulation and measurement results, respectively.

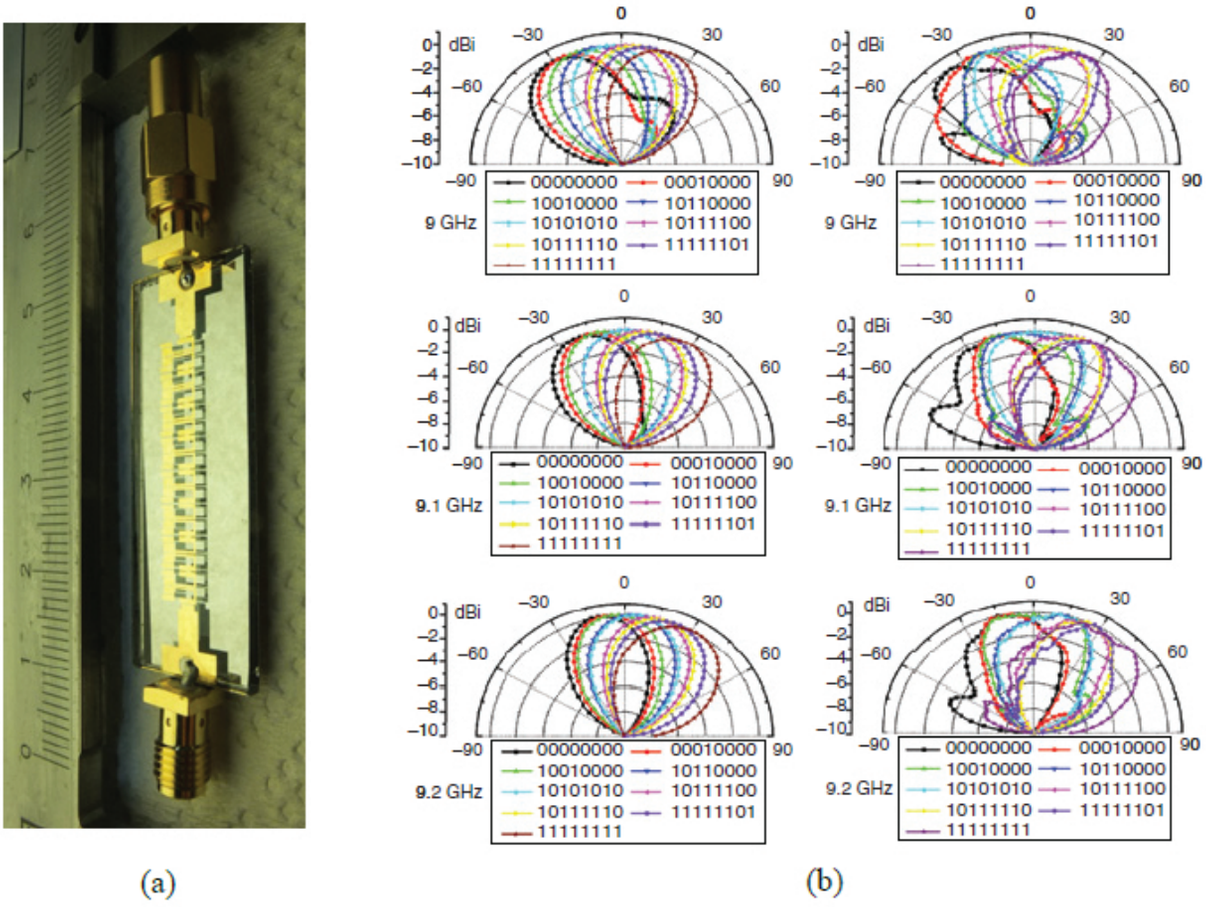

Figure 33. (a) Fabricated micromachined programmable LWA and (b) simulated and measured radiation patterns scanned with different digital states [21].

14. Conclusion

In this chapter the most significant works pertaining to CRLH LWAs have been reviewed. The most practical technology suitable for LWAs is a combination of microstrip and SIW which is compatible with integrated circuits. Also, SIW is a low loss technology which is able to carry high power. Four major beam scanning approaches were introduced which include frequency, bias voltage of a varactor, magnetic bias of a ferrite, and short/open gaps (digital states). The main characteristics of a CRLH unit cell are its dispersion diagram and Bloch impedance. The equivalent circuit of a CRLH cell comprises two capacitors and two inductors and can be implemented in many forms studied in the chapter. CRLH unit cells are not the only choice for LWAs but they have acquired a wide range of application and diversity. Leaky wave radiation is obtained based on either below-cutoff or the preferable above-cutoff waveguide operation. The LWAs can be made dual band, wideband, circularly polarized and reconfigurable. They are useful in reflecto-directive systems and can be integrated with active devices. The LWAs are promising alternatives to phase shifters which greatly reduce the cost and

complexity of the beam scanning systems. Specifically they can be conformed to the body of satellites where a simple light-weight technology becomes crucial.

Author details

Keyhan Hosseini* and Zahra Atlasbaf

*Address all correspondence to: k.hosseini@modares.ac.ir

Faculty of Electrical and Computer Engineering, Tarbiat Modares University, Tehran, Iran

References

[1] A. Oliner. Leaky Wave Antennas. In: Antennas Engineering Handbook. 3rd. ed. New York: McGraw Hill; 1993.

[2] J. D. Kraus, and R. J. Marhefka. Antennas. New York: McGraw Hill. 2001.

[3] A. Ishimaru. Electromagnetic Wave Propagation, Radiation, and Scattering. New Jersey: Prentice Hall; 1991.

[4] C. Caloz, and T. Itoh. Electromagnetic Metamaterials: Transmission Line Theory and Microwave Applications. Hoboken, NJ: Wiley intersci.; 2006.

[5] A. Sanada, C. Caloz, and T. Itoh. Characteristics of the composite right/left-handed transmission lines. IEEE Microwave and Wireless Components Letters. 2004;14(2):68–70.

[6] S. Lim, C. Caloz, and T. Itoh. Metamaterial-based electronically controlled transmission-line structure as a novel leaky-wave antenna with tunable radiation angle and beamwidth. IEEE Transactions on Microwave Theory and Techniques. 2005;53(1):161–173.

[7] Y. Dong, and T. Itoh. Composite right/left-handed substrate integrated waveguide and half mode substrate integrated waveguide leaky-wave structures. IEEE Transactions on Antennas and Propagation. 2011;59(3):767–775.

[8] F. P. Miranda, C. Penalosa, and C. Caloz. High-gain active composite right/left-handed leaky-wave antenna. IEEE Transactions on Antennas and Propagation. 2006;54(8):2292–2300.

[9] S. Lim, C. Caloz, and T. Itoh. A reflecto-directive system using a composite right/left-handed (CRLH) leaky-wave antenna and heterodyne mixing. IEEE Microwave and Wireless Components Letters. 2004;14(4):183–185.

[10] J. Machac, M. Polivka, and K. Zemlyakov. A dual band leaky wave antenna on a CRLH substrate integrated waveguide. IEEE Transactions on Antennas and Propagation. 2013;61(7):3876–3879.

[11] T. Kodera, and C. Caloz. Dual-band full-space scanning leaky-wave antenna based on ferrite-loaded open waveguide. IEEE Antennas and Wireless Propagation Letters. 2009;8:1202–1205.

[12] G. Zamora, S. Zuffanelli, F. Paredes, F. J. H. Martinez, F. Martin, and J. Bonache. Fundamental-mode leaky-wave antenna (LWA) using slotline and split-ring-resonator (SRR)-based metamaterials. IEEE Antennas and Wireless Propagation Letters. 2013;12:1424–1427;

[13] K. Hosseini, and Z. Atlasbaf. Analysis and synthesis of singly-curved microstrip structures utilizing modified Schwarz-Christoffel transformation. IEEE Transactions on Antennas and Propagation. 2013;61(12):5940–5947.

[14] K. Hosseini, and Z. Atlasbaf. Mutual coupling between two microstrip patch antennas on concave and convex cylindrical surfaces. In: Proceedings of the IEEE National Conference on Electrical Engineering (ICEE2013); 1–4 May 2013.

[15] K. Hosseini, and Z. Atlasbaf. Guided- and radiated-wave characteristics of a rectangular patch antenna located on a singly-curved surface. Progress in Electromagnetic Research C. 2013;38:205–216.

[16] K. Hosseini, and Z. Atlasbaf. Mutual coupling between two microstrip patch antennas on a singly curved surface. IEEE Antennas and Wireless Propagation Letters. 2013;12: 313–316.

[17] K. Hosseini, and Z. Atlasbaf. Design of a cylindrical CRLH leaky-wave antenna using conformal mapping. In: Proceedings of the IEEE International Symposium on Telecommunications (IST2012); 33–36 November 2012.

[18] M. Niayesh, and Z. Atlasbaf. Broadband CRLH beam-scanning LWA designed on dual-layer SIW. Applied Computational Electromagnetics Society Journal. 2016;31(4): 450–454.

[19] H. Lee, J. Choi, C. M. Wu, and T. Itoh. A compact single radiator CRLH-inspired circularly polarized leaky-wave antenna based on substrate integrated waveguide. IEEE Transactions on Antennas and Propagation. 2015;63(10): 4566–4572.

[20] Y. L. Lyn, X. X. Liu, P. Y. Wang, D. Erni, Q. Wu, C. Wang, N. Y. Kim, and F. Y. Meng. Leaky-wave antennas based on non-cutoff substrate integrated waveguide supporting beam scanning from backward to forward. IEEE Transactions on Antennas and Propagation. 2016;64(6):2155–2164.

[21] Y. Lu, K. Kikuta, Z. Han, T. Takahashi, A. Hirose, and H. Toshiyoshi. Programmable leaky-wave antenna with periodic J-shaped metamaterial patches. Electronics Letters. 2015;51(10):733–734.